Hindawi
Advances in Civil Engineering
Volume 2020, Article ID 8898433, 17 pages
https://doi.org/10.1155/2020/8898433

Research Article

Long-Term Settlement of High Concrete-Face Rockfill Dam by Field Monitoring and Numerical Simulation

Xinjie Zhou,[1] **Xinjian Sun**,[1] **Junxing Zheng**,[2] **Haoyuan Jiang**,[3] **Yongye Li**,[4] **Zhigang Li**,[4] **Zhongxiang Ma**,[4] **Peng Cao**,[5] **Qibing Zhan**,[1] **and Yawei Zhao**[1]

[1]*Qinghai University, Xining, Qinghai Province 810016, China*
[2]*Department of Civil, Construction and Environmental Engineering, Iowa State University, 354 Town Engineering Building, Ames, IA 50011, USA*
[3]*Cold and Arid Regions Water Engineering Safety Research Center, Key Laboratory of Agricultural Soil and Water Engineering in Arid and Semiarid Areas of Ministry of Education, Northwest A&F University, Yangling 712100, China*
[4]*Construction Management Bureau of the Xujixia Water Conservancy Project in Haixi Prefecture, Delingha 817000, China*
[5]*College of Architecture and Civil Engineering, Beijing University of Technology, Beijing 100124, China*

Correspondence should be addressed to Xinjian Sun; sunxj@qhu.edu.cn and Junxing Zheng; junxing@iastate.edu

Received 29 June 2020; Revised 13 October 2020; Accepted 17 October 2020; Published 7 November 2020

Academic Editor: Xinbao Yu

High concrete-face rockfill dams (CFRDs) with heights of over 100 m have been quickly developed in recent years. The self-weight of rockfill materials causes creep deformation of the dam body. However, the creep analysis method of high CFRDs in finite element software is few, and sometimes, it can also not reflect the long-term performance of high CFRDs well. Therefore, it is necessary to carry out the secondary development in finite element software. This study developed a subroutine that can run in Finite Element Method (FEM) platform ABAQUS to simulate long-term creep deformation behavior of the rockfill materials more accurately. Then, a displacement back-analysis for parameters, based on the Xujixia high CFRD project, is performed by the neural network response surface method (BP-MPGA/MPGA). Remarkable agreements are observed between simulation and field monitoring results. The calibrated FEM model is used to predict stress and deformation behavior of the Xujixia high CFRD after three years of operation period. The result indicates that rockfill creep deformation has a significant impact on stress and deformation of the high CFRD during the operation. This research may predict long-term performance using FEM in the design stage for high CFRDs.

1. Introduction

Concrete-face rockfill dams (CFRDs) have been quickly developed in recent years because of the adaptability to terrain, low cost, and facilitated construction [1]. However, researchers have observed creep deformation of rockfills in the body of high CFRDs even under normal operating conditions [2–6]. The creep can cause differential and inconsistent deformation between rockfill and concrete-face, resulting in detachment of these two structural elements [7, 8]. Without the support of rockfill, fractures may develop in concrete-face panels caused by panel's weight and external loads, which seriously affects the performance and fatigue life of CFRDs [9]. For example, the fractured concrete-faces have been reported in the Australian Cethana CFRD with a height of 110 m and the Chinese Tianshengqiao CFRD with a height of 178 m. If the fractures continue to develop, significant water leaks may occur [10, 11], which may cause structural failure of the dams [12–18], such as Gouhou CFRD failure in August 1993 in Qinghai Province, China [19].

Finite Element Method (FEM) has demonstrated advantages for predicting the mechanical performance of dams for better management and maintenance [20–27]. The FEM

can also provide useful guidance for the design and construction of new high CFRDs by optimizing dam body structures, construction procedures, and dam construction materials [8]. In order to obtain the creep model of rockfill for FEM simulations, researchers have conducted large-scale triaxial tests for investigating the time-dependent behavior of coarse granular materials under different stress paths, confining pressures, and moisture contents [28–37]. The analyses reveal that creep deformation of the rockfill is caused by stress redistribution in the dam body associated with a process of abrasion of sharp corners of stones, particle shape, and particle breakage [38–44].

According to triaxial test results, theoretical models have been developed to characterize the creep behavior of rockfill materials. Theoretical models mainly use elastic elements (linear springs), viscous elements (Newton's stick pots), and plastic elements (friction parts) to form series and parallel connections to describe time-dependent stress-strain relationship of rockfill materials. Based on the combination and expansion of the above three elements, a variety of theoretical models for evaluating creep behavior of rockfill materials have been proposed [45, 46], such as Merchant model, viscoelastic model, elastic-viscoplastic model, elastoplastic model, and Hardening Soil Creep (HSC) model [40, 47–52]. Theoretical models are supported by rigorous mathematical theory, which is very important for investigating the mechanical characteristics of rockfill materials. The results of large-scale triaxial tests can be used to determine theoretical model parameters. However, the large-scale triaxial tests are subject to sample disturbance and size effects, and the theoretical model parameters are limited by undefined practical meaning [31, 53–56]. Therefore, indoor creep test results often have a large divergence with actual creep measurements in the field [57, 58]. As such, empirical models are developed by assessing field monitoring data of CFRDs. Statistical methods are used to analyze creep deformation curve to obtain empirical model functions, such as exponential decay function, hyperbolic type function, and power function [29, 59, 60]. In order to better understand the dam deformation property, it is necessary to conduct deformation monitoring analysis, empirical model, and back-analysis.

This case study focuses on the field monitoring results of Xujixia high CFRD (121.5 m) and developing a subroutine in ABAQUS using exponential decay-type empirical creep model to evaluate creep deformation of high CFRDs. The simulation parameters were determined based on displacement back-analysis (BP-MPGA/MPGA) considering the construction process and field compaction test results. The effectiveness of the proposed method is validated by field monitoring results of Xujixia high CFRD.

2. Establishment of the Creep Model in ABAQUS

2.1. Creep Model. Field monitoring results of Xujixia high CFRD show that the rockfill creep deformation increment decreases with time and can be simulated using a Merchant model [61], which is expressed as follows:

$$\varepsilon^{\mathrm{cr}}(t) = \varepsilon_f\left(1 - \exp^{-at}\right), \tag{1}$$

where $\varepsilon^{\mathrm{cr}}$ is time-dependent creep strain, ε_f is final creep deformation when $t \longrightarrow \infty$, a is the ratio of initial creep deformation when $t = 0$, and exp is the base of natural logarithm.

Therefore, strain rate can be computed as

$$\dot{\varepsilon}^{\mathrm{cr}} = a\varepsilon_f \exp^{-at}. \tag{2}$$

Assuming that creep deformation of the rockfill is related to confining pressure and stress level, total creep deformation of the rockfill can be divided into volume creep $\varepsilon_{\mathrm{vf}}$ depending on confining pressure and shear creep $\varepsilon_{\mathrm{sf}}$ depending on stress level. According to the rockfill and clay creep deformation test results, Shen et al. [62, 63] determined that volumetric creep deformation and shear creep deformation could be simulated as

$$\varepsilon_{vf} = b\frac{\sigma_3}{P_a}, \tag{3}$$

$$\varepsilon_{sf} = d\frac{D}{1-D}. \tag{4}$$

Based on the rockfill creep deformation test results, Li et al. [64] updated equations (3) and (4) to incorporate the shear stress influence on final shear creep deformation to reflect the influence of particle breakage on creep deformation. The updated equations (3) and (4) are expressed as

$$\begin{aligned} \varepsilon_{vf} &= b\left(\frac{\sigma_3}{P_a}\right)^{m_1} + c\left(\frac{q}{P_a}\right)^{m_2}, \\ \varepsilon_{sf} &= d\left(\frac{D}{1-D}\right)^{m_3}, \end{aligned} \tag{5}$$

where b and d are two model parameters. b is equivalent to final volume creep at $\sigma_3 = P_a$ (atmospheric pressure), with a stress level $D = (\sigma_1 - \sigma_3)/(\sigma_1 - \sigma_3)_f$. Specifically, σ_1 is the major principal stress, and σ_3 is the minor principal stress. d is final shear creep at stress level $D = 0.5$. When FEM is used for creep analysis, the range of stress level significantly affects the results of creep calculation. Therefore, stress level should be reasonably limited based on the actual situation, where a, b, c, d, m_1, m_2, and m_3 are model parameters.

Based on the Prandtl–Reuss flow rule, the uniaxial creep rate can be obtained after three-dimensional creep rate is degraded [65]. Therefore, the creep rate of each component of strain tensor can be written as

$$\{\dot{\varepsilon}^{\mathrm{cr}}\} = \frac{1}{3}\dot{\varepsilon}_v\{I\} + \frac{3\dot{\varepsilon}_s}{2\sigma_s}\{S\}, \tag{6}$$

where $\{S\}$ is the partial stress, $\{I\}$ is the unit tensor, and σ_s is the generalized shear stress. The volumetric deformation rate $\dot{\varepsilon}_v$ and the shear deformation rate $\dot{\varepsilon}_s$ are

$$\begin{aligned} \dot{\varepsilon}_v &= a\varepsilon_{vf}\exp^{-at}, \\ \dot{\varepsilon}_s &= a\varepsilon_{sf}\exp^{-at}. \end{aligned} \tag{7}$$

CFRDs are filled in phases and zones; the loading process is complicated. The specific initial creep occurrence time of a cast layer and the subsequent creep occurrence time after the stress state changes are difficult to accurately determine. So, as an implementation of incremental creep routines in ABAQUS, relative time is used for creep calculations. Thus, the volume deformation rate and shear deformation rate can be changed to

$$\dot{\varepsilon}_v = \begin{cases} 0, & \varepsilon_{vf} = 0, \\ a\varepsilon_{vf}\left(1 - \dfrac{\varepsilon_{vt}}{\varepsilon_{vf}}\right), & \varepsilon_{vf} \neq 0, \end{cases} \tag{8}$$

$$\dot{\varepsilon}_s = \begin{cases} 0, & \varepsilon_{sf} = 0, \\ a\varepsilon_{sf}\left(1 - \dfrac{\varepsilon_{st}}{\varepsilon_{sf}}\right), & \varepsilon_{sf} \neq 0. \end{cases} \tag{9}$$

For rockfill materials subject to zero stress, $\varepsilon_{vf} = \varepsilon_{sf} = 0$ according to equations (3) and (4), where ε_{vf} and ε_{sf} are the accumulated volume and shear creep variables for time t, which can be calculated as in the following equations by integration:

$$\varepsilon_{vt} = \sum \dot{\varepsilon}_v \Delta t, \tag{10}$$

$$\varepsilon_{st} = \sum \dot{\varepsilon}_s \Delta t. \tag{11}$$

The creep strain increment tensor $\{\Delta\varepsilon^{cr}\}$ can be obtained according to equations (6), (8), and (9):

$$\{\Delta\varepsilon^{cr}\} = \left(\frac{1}{3}\dot{\varepsilon}_v\{I\} + \frac{3\dot{\varepsilon}_s}{2\sigma_s}\{S\}\right)\Delta t. \tag{12}$$

Thus, subroutine is written in FEM platform ABAQUS through the above incremental creep model ($\{\Delta\varepsilon^{cr}\}$).

2.2. Implementation of Creep Model in ABAQUS. The creep model in Section 2.1 is implemented in finite element program ABAQUS through the user-defined material subroutine (UMAT) as shown in Figure 1. Therefore, the creep model needs to be written in incremental form, and the stress increment tensor $\{\Delta\sigma(t_n)\}$ is expressed as

$$\{\Delta\sigma(t_n)\} = [D]\{\Delta\varepsilon^{el}\}, \tag{13}$$

where $[D]$ is the elastic stiffness matrix, also called the Jacobian matrix; $\{\Delta\varepsilon^{el}\}$ is the elastic strain increment tensor.

The total strain increment includes an elastic strain increment tensor and a creep strain increment tensor. The elastic strain increment tensor is

$$\{\Delta\varepsilon^{el}\} = \{\Delta\varepsilon\} - \{\Delta\varepsilon^{cr}\}, \tag{14}$$

where $\{\Delta\varepsilon\}$ is the total strain increment tensor (DSTRAN); $\{\Delta\varepsilon^{cr}\}$ is the creep strain increment tensor.

The finite element calculation process is divided into filling stage during construction and creep stage during operation by analyzing step KSTEP. The calculation process of ABAQUS with UMAT-based creep model includes five steps: (1) determine initial stress state of creep; (2) determine the beginning of the creep stage; (3) determine the creep strain increment tensor; (4) determine the stress increment tensor; and (5) update the stress tensor, the Jacobian matrix, and state variable (STATEV).

The subroutine compiled by Fortran is used to implement exponential decay-type empirical creep model. With FEM software ABAQUS, the stress and deformation simulation analysis, considering rockfill creep, was performed for the Xujixia CFRD.

3. The Xujixia CFRD

The Xujixia CFRD Project, as shown in Figure 2(a), is one of the 172 major water projects identified by the State Council of China. It is located about 6 km upstream of the Bayin River Canyon Exit and approximately 60 km northeast of Delingha City, Qinghai Province, China. Specifically, the maximum height of dam is 121.5 m, and the altitude of dam crest is 3472.0 m. The width of dam crest is 8 m, and the length of dam crest is 365.0 m. The upstream slope is 1:1.4, and the downstream composite slope is 1:1.85. The normal water storage level of reservoir is 3468.00 m, and the total storage capacity of reservoir is 162 million m3. The total volume of dam filling materials is 4,185,500 m^3 (see Table 1). The rockfill materials are primary rockfill (3B) and secondary rockfill (3C). The primary rockfill is a mixture of sandstone and sandy slate with low compressibility and high shear strength. The secondary rockfill is a mix of slate and riverbank gravel at the dam construction site. Figures 2(b) and 2(c) show the plan view and cross section of the Xujixia CFRD.

A total of 35 extensometers are used to monitor the internal settlement of dam at five altitudes of 3392, 3395, 3425, 3430, and 3433 m at three observation sections of D0 + 083.8, D0 + 163.8, and D0 + 223.8 m as shown in Table 2. Figures 2(b) and 2(c) show locations of extensometers.

The dam is constructed in multiple phases as shown in Figure 2(d). The tests, as shown in Table 3, are performed on dam filling materials to determine the mechanical properties before and after compaction. The results are shown in Table 4 and Figure 3. After roller compaction, the maximum particle size of the rockfill is reduced from 800 mm to 600 mm. The percentage of the particles with a size of $D < 5$ mm increases from 15.73% to 16.38%. The fine particles with size of $D < 0.075$ mm increase from 0.84% to 1.61%. The dry density increases from the 1.92 g/cm^3 to 2.18 g/cm^3. These index test results meet the design values. It is observed that the weak particles and sharp edges of the particles are broken during the compaction process.

Based on particle size distribution curves in Figure 3, the particle breakage of rockfill materials mainly occurs for particles in a size range of 300 mm–800 mm, resulting in the reduced particle size and increased percentage of fine

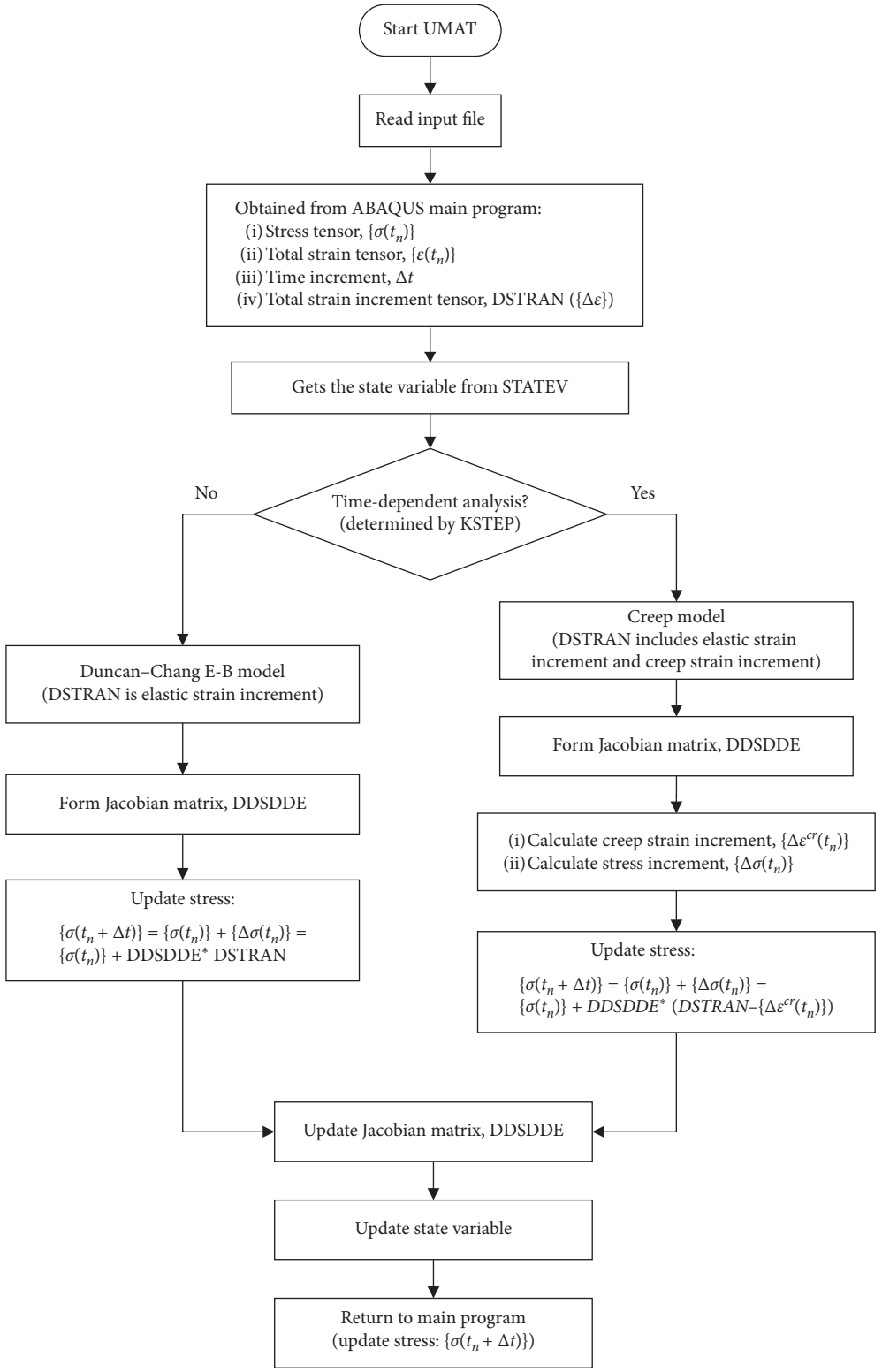

Figure 1: The UMAT algorithm flowchart for creep analysis in ABAQUS.

particles. These broken particles are rearranged to fill the voids between large particles. Therefore, the dry density, the compactness, and the compressive strength of rockfill are increased. After compaction, the porosity of rockfill material is 19.1%, and the permeability coefficient is 1.75×10^{-1} cm/s.

The settlement period of dam before water storage is mainly affected by the creep deformation of rockfill rather than the external water pressure. Therefore, settlement monitoring data are used to evaluate the effectiveness of the creep subroutine in ABAQUS.

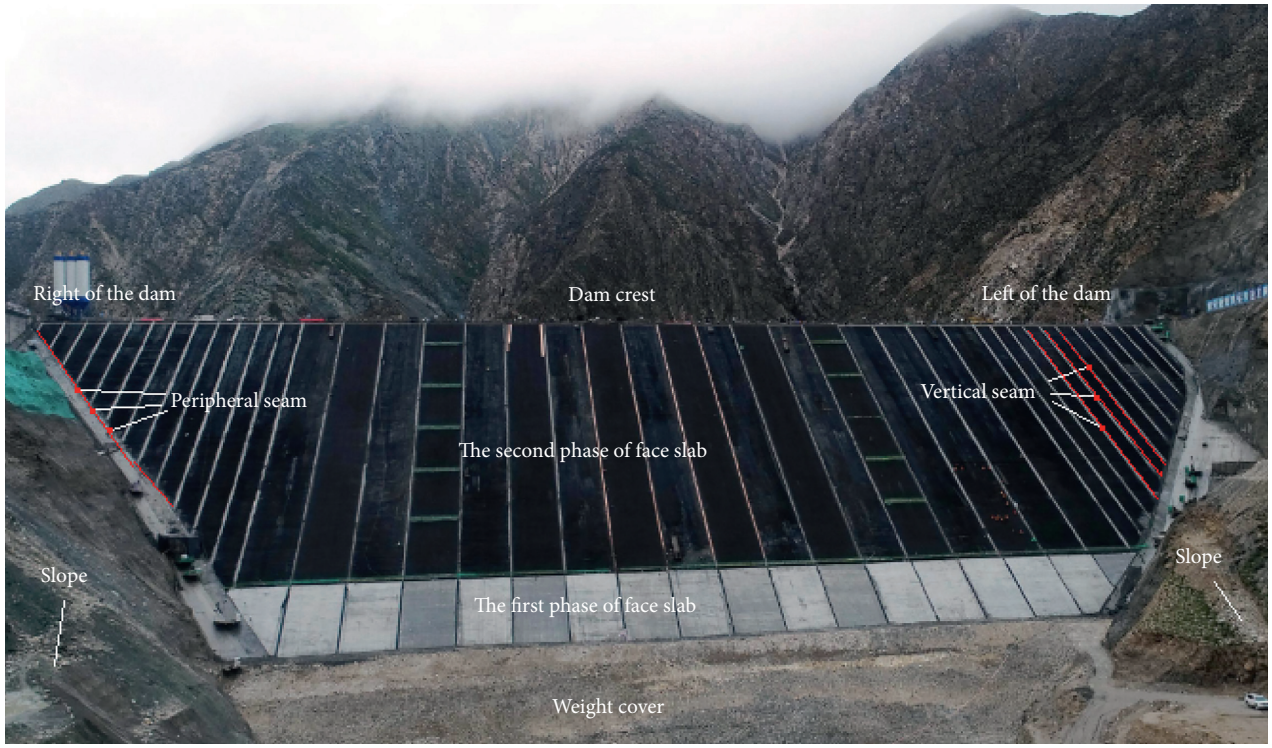

(a)

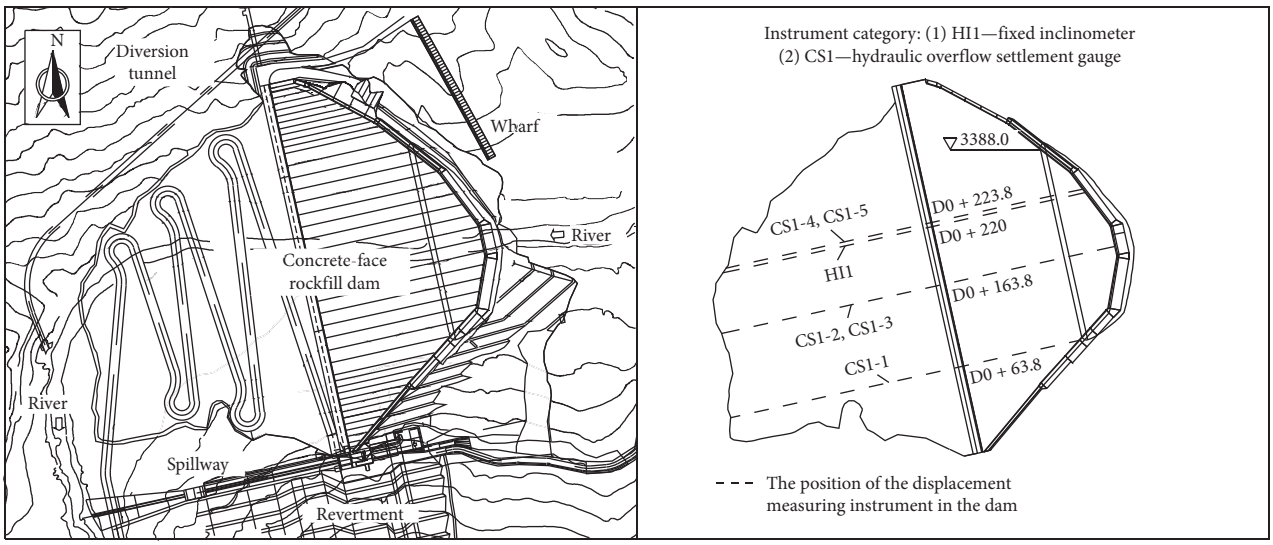

(b)

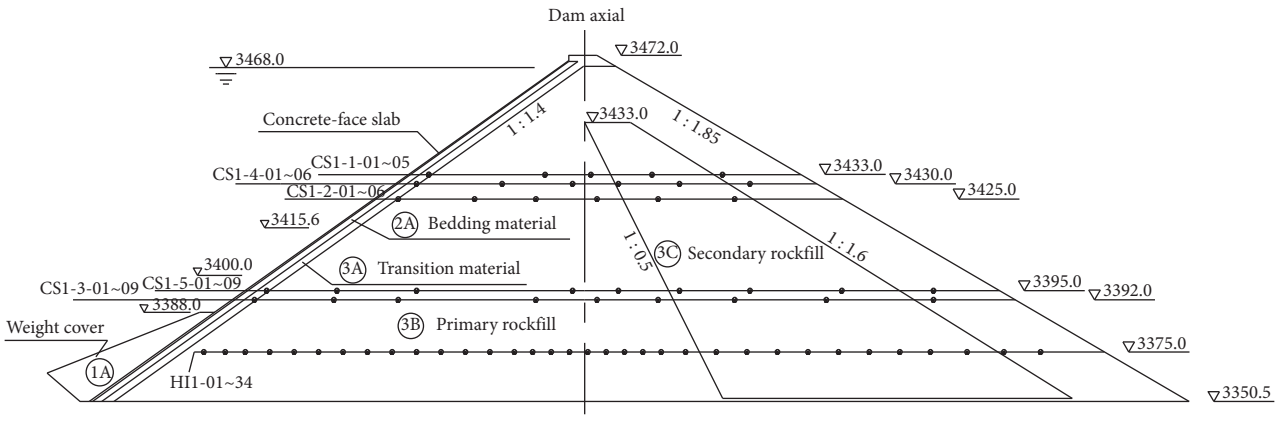

(c)

Figure 2: Continued.

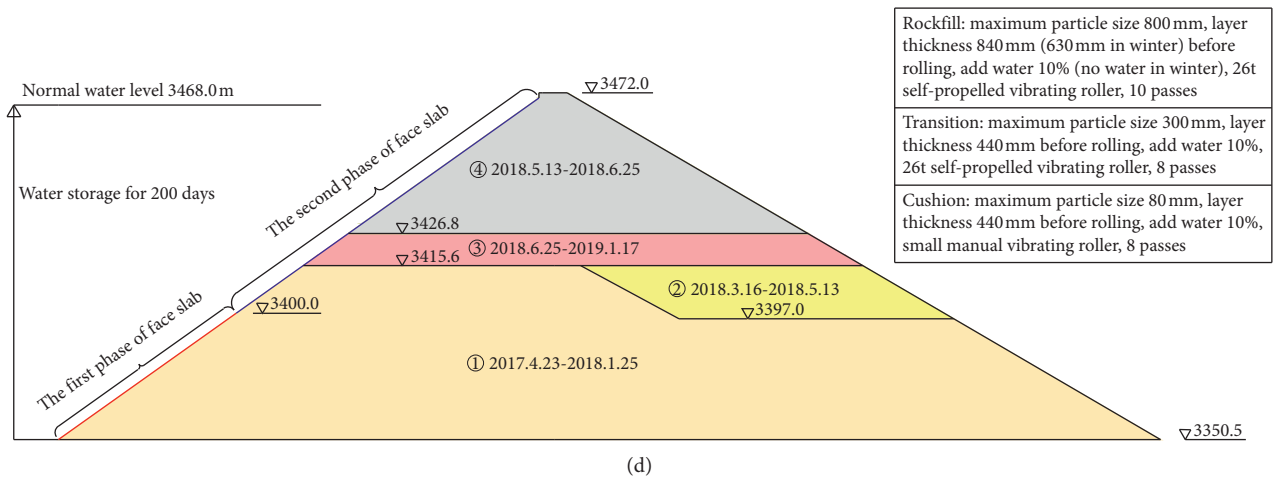

Figure 2: The overview of the Xujixia CFRD project. (a) The Xujixia CFRD. (b) The plan view of the Xujixia CFRD and locations of extensometers. (c) The cross section of the Xujixia CFRD and locations of extensometers. (d) The construction phases of Xujixia CFRD.

Table 1: The filling amount of rockfill materials for the Xujixia rockfill dam.

Dam-filling material	Filling amount (m^3)
All dam-filling materials	4,185,500
Dam front gland 1A	66,300
Cushion material 2A	109,200
Transition material 3A	241,700
Main rockfill 3B	2,611,100
Secondary rockfill 3C	1,157,200

Table 2: The arrangement of extensometers.

Section	Altitude (m)	Numbers of measuring points	Device number (from upstream to downstream)
Left of the dam D0 + 83.8 m	3433	5	CS1-1-01~CS1-1-05
Left of the dam D0 + 163.8 m	3425	6	CS1-2-01~CS1-2-06
Left of the dam D0 + 223.8 m	3392	9	CS1-3-01~CS1-3-09
	3430	6	CS1-4-01~CS1-4-06
	3395	9	CS1-5-01~CS1-5-09

Table 3: Mechanical properties tests of dam filling materials.

Measurement basis	Measurement items	Tests
≪Geotechnical test method standard≫ SL 237–1999 (current standard for water conservancy projects in China)	Particle gradation	The new national standard soil sieve (particle size: 0.075–5 mm)
		Hand-carried coarse-grained soil sieve (particle size: 5–200 mm)
		Ruler (particle size: 200–800 mm)
	Porosity (using the weighted average method based on the particle gradation)	Pycnometer (particle size: less than 2 mm)
		Hydrometer (particle size: more than 2 mm)
	Permeability coefficient (noncohesive)	Constant head test

4. Three-Dimensional Numerical Calculation

4.1. Model Introduction. A three-dimensional FEM model is built for simulating the Xujixia CFRD as shown in Figure 4(a). The Xujixia CFRD body consists of 20921 elements, 8-node hexahedral elements. At boundary transitions, prismatic elements are utilized. The vertical and horizontal displacement at the bottom are fixed. The thickness of panel is between 0.4 m and 0.81 m. Goodman contact elements [66, 67] without thickness are applied between panel and rockfill. Figure 4(b) is a two-dimensional model of standard cross section of the Xujixia CFRD based on phased and zoned construction as shown in Figure 2(d). The model is divided into 645 elements, including 60 transitional elements. The dam body is simulated according to the actual construction process, and the dam body is filled in four phases. The first phase is divided into 11 layers for full cross section and front-dam horizontal filling to altitude 3415.6 m and the first phase of panel construction to altitude 3400 m; the second phase is divided into 4 layers for postdam horizontal filling to altitude 3415.6 m; the third phase is divided into 2 layers for full cross section horizontal filling to altitude 3426.8 m; and the fourth phase is divided into 10 layers for full cross section horizontal filling to altitude 3472.0 m and the second phase of panel construction to altitude 3470.0 m. In ABAQUS, the birth-death element (model change) and Duncan–Chang E-B model are used to implement the phased and zoned construction of the Xujixia CFRD.

Table 4: Mechanical properties tests results of rockfill materials.

Material	Roller compaction				Particle size (D)					Dry density (g/cm^3)	Porosity (%)	Hydraulic conductivity (cm/s)	Saturated compressive strength (cm/s)
	Layer thickness (cm)		Times of roller compaction	Rolling settlement (cm)	Maximum particle size (D/mm)	The content of $D < 5$ mm		The content of $D < 0.075$ mm					
	Before rolling (cm)	After rolling (cm)				Raw material (%)	After rolling (%)	Raw material (%)	After rolling (%)				
Rockfill	84	80.5	10	3.5	$D < 800$	15.73	16.38	0.84	1.61	2.18	19.1	1.75×10^{-1}	81
Transition	44	41	8	3.0	$D < 300$	18.62	19.63	2.63	3.15	2.21	16.8	1.89×10^{-2}	81
Cushion	44	40.8	8	3.2	$D < 80$	40.5	38.2	4.4	5.2	2.25	12.3	1.05×10^{-2}	89

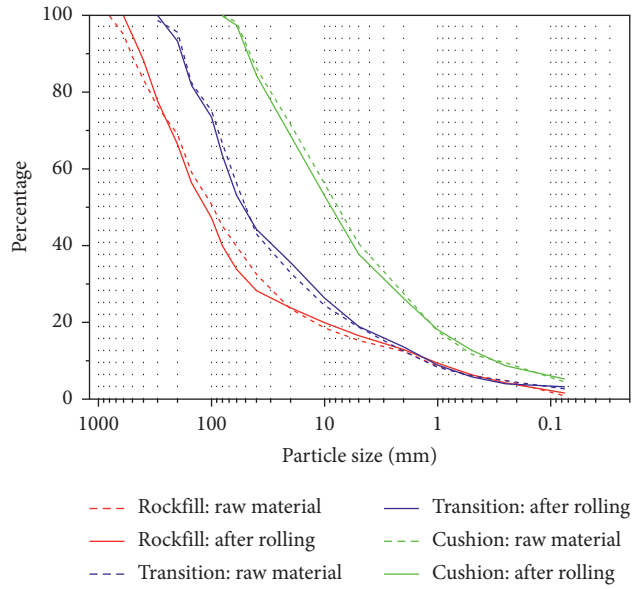

Figure 3: Particle gradation curve of compaction test.

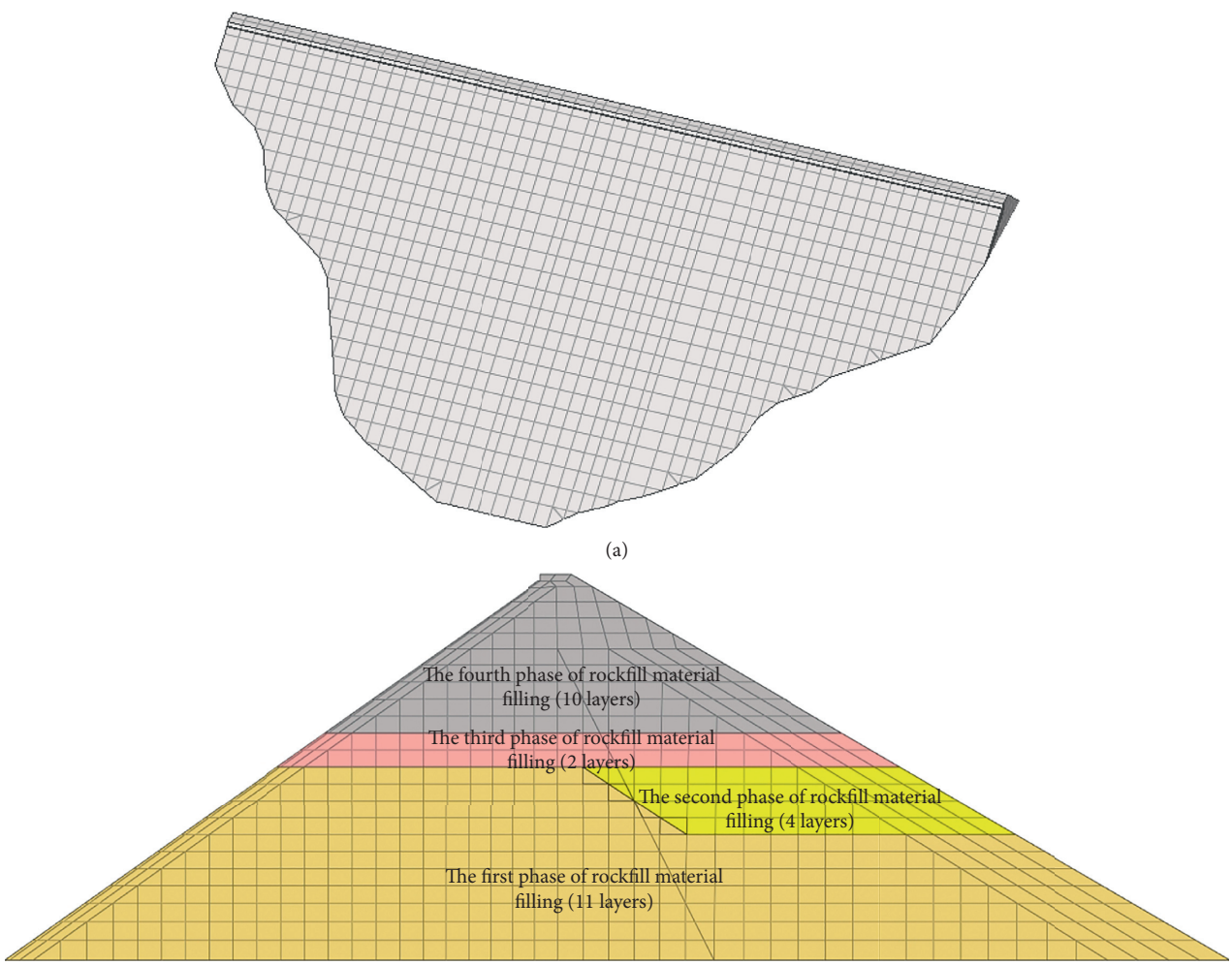

Figure 4: The model of the Xujixia CFRD. (a) Three-dimensional finite element grid. (b) Standard cross section finite element grid.

Figure 5: ST-1500-type electrohydraulic servo static triaxial tester.

Table 5: Duncan–Chang E-B model calculation parameters.

Dam-filling material	Dry density ρ_d/(g/cm^3)	E-B model parameters						
		ϕ_0	$\Delta\phi$	R_f	K	n	K_b	m
Main rockfill	2.13	53	10	0.86	1022	0.32	465	0.10
Secondary rockfill	2.11	45	8	0.80	863	0.26	338	0.02
Cushion material	2.23	50	7	0.76	1150	0.35	480	0.25
Transition material	2.25	48	7	0.70	1090	0.35	450	0.23

ϕ_0 = the internal friction angle when the confining pressure is one atmosphere, $\Delta\phi$ = the internal friction angle that changes with pressure, R_f = the failure ratio, K = the tangent modulus coefficient, n = the tangent modulus index, K_b = volume modulus coefficient, and m = bulk modulus index.

4.2. Determination of Simulation Parameters

4.2.1. Linear Elastic Model. A linear elastic model was used to characterize the mechanical properties of the concrete panel, with an elastic modulus of 30 GPa and a Poisson ratio of 0.167.

4.2.2. Duncan–Chang E-B Model and Creep Model. The Duncan–Chang E-B model is used to characterize the nonlinear stress-strain relationship of the rockfill.

The tangent modulus E_t in the model can be expressed as

$$\begin{cases} E_t = \left(1 - R_f S\right)^2 \cdot K \cdot P_a \cdot \left(\dfrac{\sigma_3}{P_a}\right)^n, \\ S = \dfrac{(1 - \sin\phi)(\sigma_1 - \sigma_3)}{2C.\cos\phi + 2\sigma_3 \sin\phi}. \end{cases} \tag{15}$$

Nonlinear volume change can be expressed as

$$B = K_b \cdot P_a \cdot \left(\frac{\sigma_3}{P_a}\right)^m. \tag{16}$$

According to the Mohr–Coulomb criterion, the friction angle of dam rockfill can be expressed as

$$\phi = \phi_0 - \Delta\phi \cdot \log\left(\frac{\sigma_3}{P_a}\right). \tag{17}$$

The rockfill test samples in this paper are from main rockfill zone and secondary rockfill zone of the Xujixia CFRD. The samples are prepared according to the gradation after scaling and designed dry density. The rockfill sample has a diameter of 300 and a height of 600 mm. The maximum particle diameter is 60 mm. The consolidated drained triaxial tests are performed on rockfill samples using a ST-1500-type electrohydraulic servo

Table 6: Creep model parameters of the rockfill.

Dam-filling material	a	b	c	d	m_1	m_2	m_3
Main rockfill/transition material/cushion material	0.0057	0.00059	0.00025	0.00298	0.637	0.652	0.631
Secondary rockfill	0.00641	0.00051	0.00043	0.00233	0.63	0.533	0.539

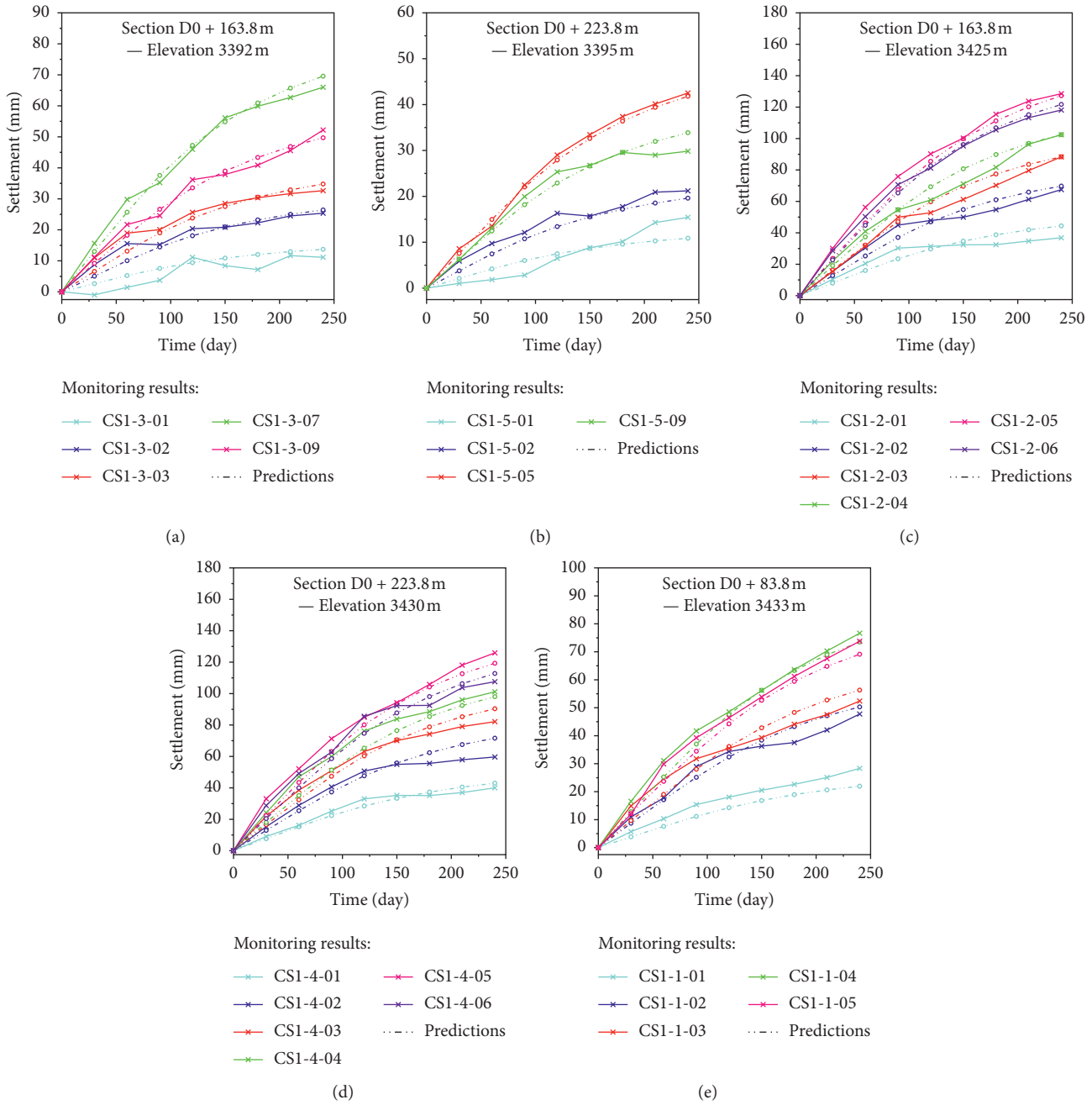

Figure 6: Comparison of the prediction and the monitoring results of settlement model in monitoring points within eight months after the completion of the Xujixia CFRD.

static triaxial test system as shown in Figure 5. Four confining pressures, 500, 1000, 1500, and 2000 kPa, are used in tests. The initial values of Duncan–Chang E-B model parameters are obtained based on the testing results and used for subsequent parameter inversion [68, 69].

The parameters of rockfill materials used in Xujixia CFRD were back-analyzed using neural network response surface method (BP-MPGA/MPGA). The inversion problem is transformed into a constraint problem. The optimization objective function is as follows:

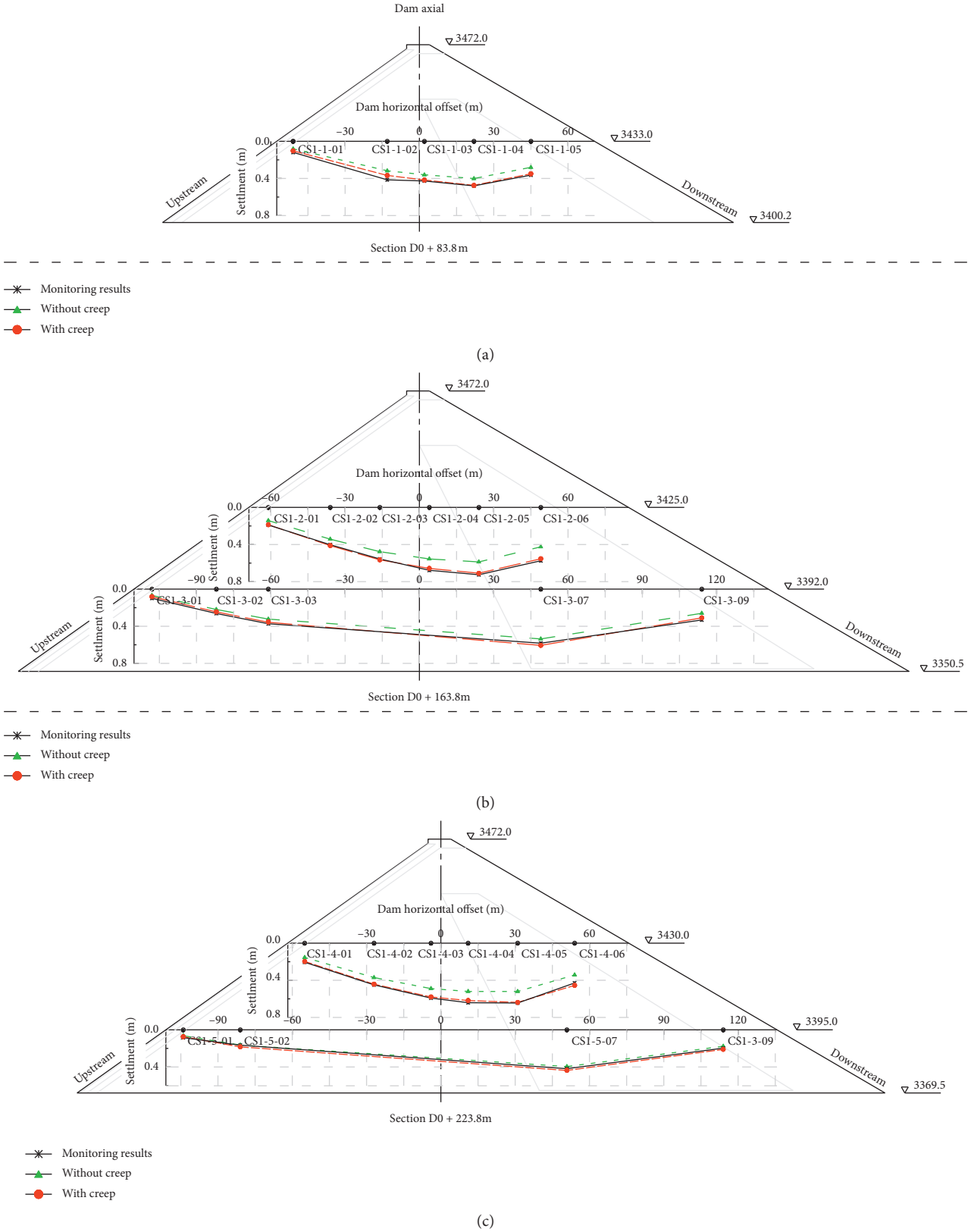

Figure 7: Comparison of dam body settlement eight months before and after the completion of filling (CS1 instruments).

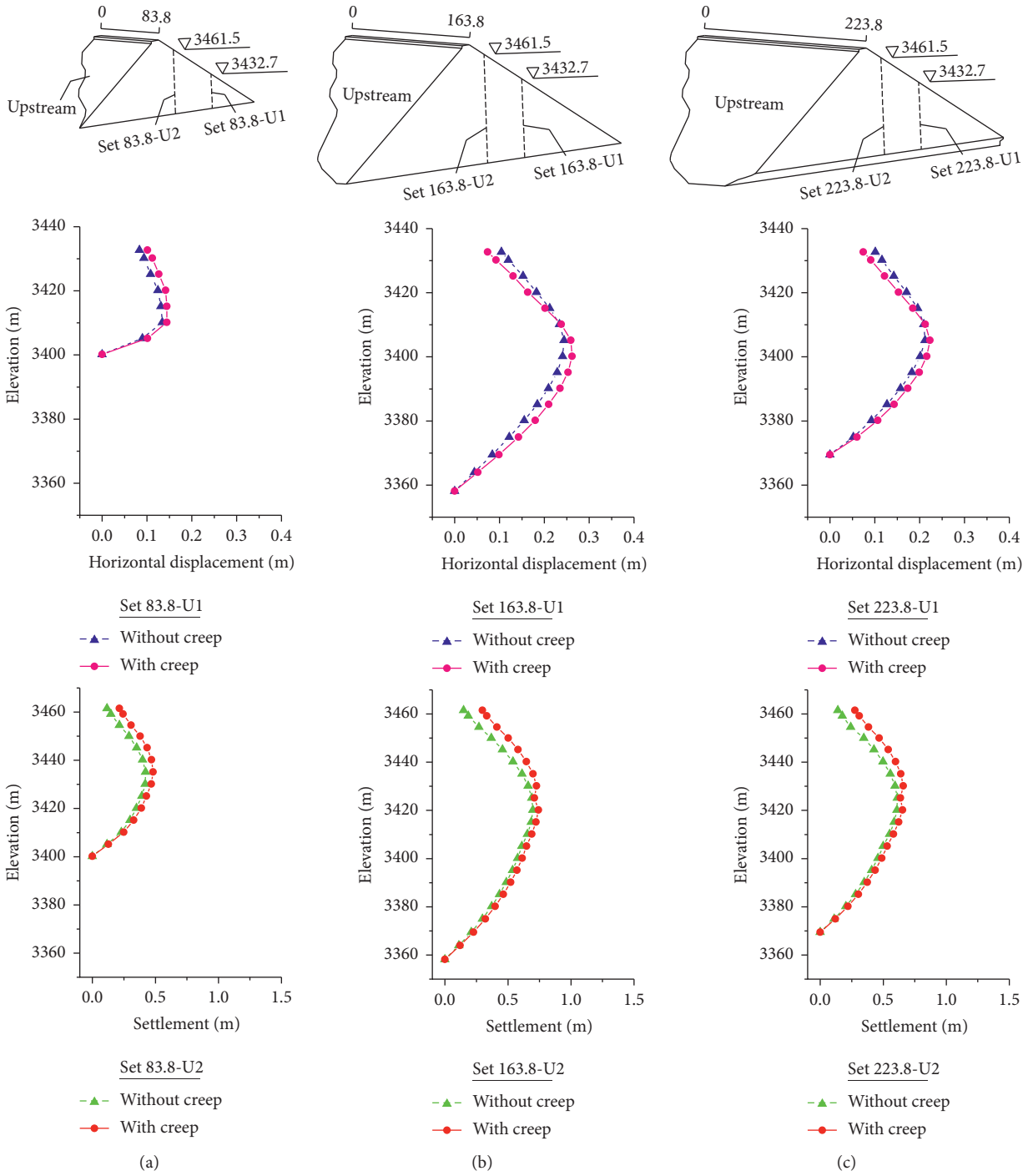

Figure 8: Horizontal displacement and settlement by FEM simulations.

$$\begin{cases} \min \quad F(X) = \sum_{i=1}^{g} W_i^{(u)} \left[\sum_{j=1}^{h} W_{ij}^{(v)} \left(\dfrac{U_{ij}^{(X)}}{U_{ij}^{\text{real}}} - 1 \right)^2 \right] \\ \text{s.t.} \quad K(X)\{U\} = \{R\} \\ \quad\; x_d^{\min} \le x_d \le x_d^{\max} \, (d = 1, 2, \ldots, D), \end{cases} \tag{18}$$

where X (D is the number of parameters to be inverted) is a group of rockfill model parameters to be inverted; $U_{ij}^{(X)}$ and U_{ij}^{real} are the calculated displacement and the monitoring displacement, respectively, at the jth displacement in the ith time period; u is the number of external environmental factors affected by the measuring point; $W_i^{(u)}$ is the weight of the external environmental factor u in the ith time period, $\sum_{i=1}^{g} W_i^{(u)} = 100$, $W_i^{(u)} = 1/u\,(W_i^{(1)} + W_i^{(2)} + \cdots + W_i^{(u)})$; v is the number of internal environmental factors affected by the

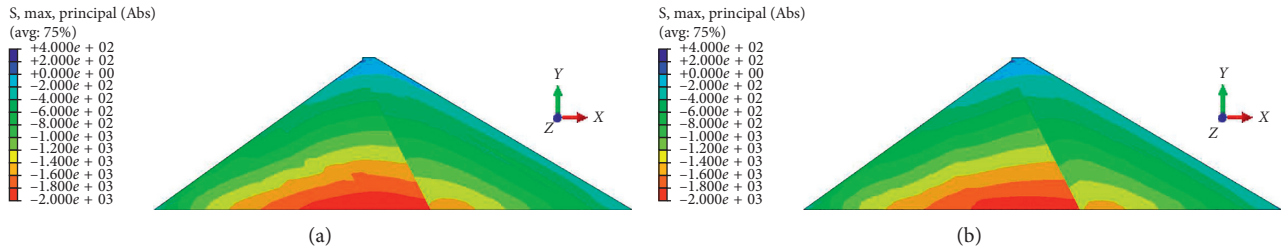

Figure 9: Major principal stress nephogram at section D0 + 163.8 after 3 years of water storage. (a) Without creep. (b) Creep.

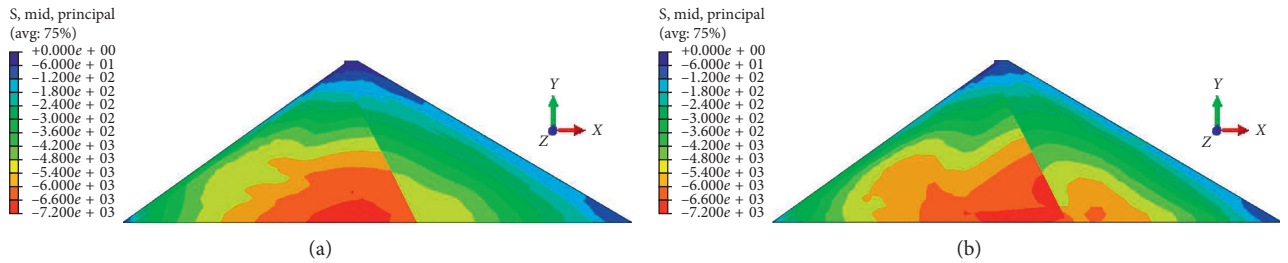

Figure 10: Minor principal stress nephogram at section D0 + 163.8 after 3 years of water storage. (a) Without creep. (b) Creep.

Table 7: Maximum simulated calculation results.

Items	Without creep		With creep		
	AC + 8 m	WSP/AWS + 3a	AC + 8 m	WSP	AWS + 3a
Settlement (m)	0.742	0.752	0.779	0.797	0.816
Horizontal displacement towards upstream (m)	0.091	0.004	0.086	0.027	0.018
Horizontal displacement towards downstream (m)	0.258	0.322	0.243	0.277	0.275
Major stress, σ_1 (MPa)	1.886	1.998	1.814	1.916	1.931
Minor stress, σ_3 (MPa)	0.658	0.698	0.671	0.712	0.706

AC + 8 m = eight months after completion, WSP = water storage period, AWS + 3a = 3 years after water storage, and with creep: consider the creep of the dam body during the settlement period and operation period.

measuring point; and $W_{ij}^{(v)}$ is the weight of the internal environmental factor v at the jth displacement in the ith time period, $\sum_{j=1}^{h} W_{ij}^{(v)} = 100$, $W_{ij}^{(v)} = 1/v(W_{ij}^{(1)} + W_{ij}^{(2)} + \cdots + W_{ij}^{(v)})$. The weight of each displacement in every time period is the same; $K(X)$, $\{U\}$, and $\{R\}$ are the stiffness matrix, node displacement array, and equivalent nodal load array; $x_d^{\min}$ and $x_d^{\max}$ are the lower and upper limits of the dth parameter of the inversion.

The lithology of cushion and transition material are close to main rockfill and there are no effective monitoring points; only the parameters of main and secondary rockfill in this paper are inversed. The Duncan–Chang E-B model parameters (Table 5) and creep model parameters (Table 6) of rockfill materials of the dam are determined through back-analysis using neural network response surface method (BP-MPGA/MPGA).

5. Analysis of Calculation Results

5.1. Comparison of Calculation Results with Monitoring Results. The simulation and monitoring results are compared in Figure 6, which agree with each other very well. The settlement rate of each measurement point gradually slows down with time. The measurement points located in sub-rockfill area (such as CS1-1-04, CS1-2-05, CS1-3-07, CS1-4-05, and CS1-5-07) have larger creep values.

Figure 7 shows the computed settlements in measured points with and without considering the dam creep. When considering creep, the calculated settlement is more consistent with the actual field monitoring results.

5.2. Creep Analysis for the Xujixia CFRD. The simulated horizontal displacement and settlement with and without considering creep are shown in Figure 8. Considering creep in simulations, larger horizontal displacement is observed.

Figures 9 and 10 show stress nephogram with and without considering creep in simulations. The maximum value of major principal stress (σ_1) at D0 + 163.8 cross section decreased from 1.996 MPa to 1.930 MPa, and the difference of principal stress ($\sigma_1 - \sigma_3$) decreased from 1.928 MPa to 1.860 MPa considering creep. The model considering creep can capture stress redistribution in the dam caused by particle breakage and rearrangement. In addition, the results indicate that the deformation of rockfill

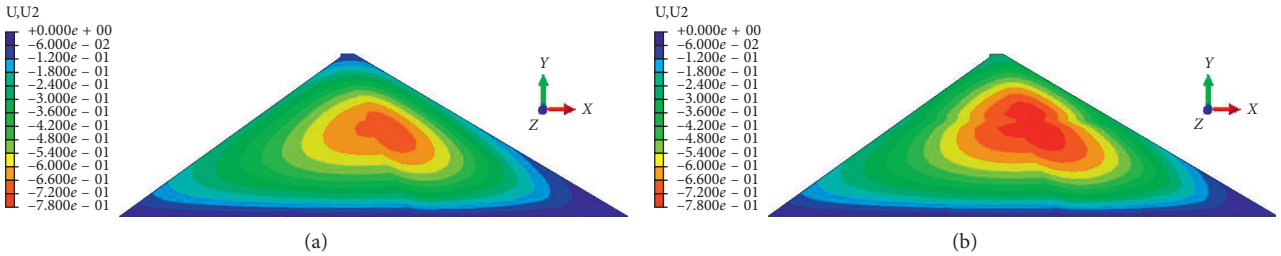

Figure 11: Settlement nephogram at section D0 + 163.8 after 3 years of water storage. (a) Without Creep. (b) Creep.

Table 8: The displacement monitoring table of typical high face rockfill dams.

Name	Country	Year	Surveyed period (year)	Height (m)	Internal settlement (operation period)	
					Settlement (m)	The percentage of the height (%)
Nalan	China	2005	6	109	0.31	0.28
Alto Anchicaya	Columbia	1974	10	140	0.63	0.45
Jilintai-1	China	2006	1	157	0.73	0.46
Chahanwushu	China	2009	2	110	0.53	0.48
Sethana	Australia	1971	10	110	0.56	0.51
Bashan	China	2008	1	155	0.83	0.54
Zipingpu	China	2003	2	156	0.88	0.56
Tankeng	China	2008	7	162	0.96	0.6
Xujixia	China	2019	3	121.5	0.816	0.67
Shanxi	China	2000	6	132.5	0.95	0.72
Hongjiadu	China	2005	2	179.5	1.32	0.74
Miaojiaba	China	2011	1	110	0.91	0.83
Jiudiaxia	China	2008	3	136	1.24	0.91
Aguamilpa	Mexico	1993	—	186	1.70	0.91
Kolan	Thailand	1985	—	130	1.20	0.92
Malutang phase II	China	2009	2	154	1.50	0.97
Duonuo	China	2012	2	112.5	1.10	0.98
Bakun	Malaysia	2008	—	203.5	2.16	1.06
Shuibuya	China	2008	3	233.2	2.50	1.07
Dongjing	China	2010	4	150	2.07	1.38
Tianshengqiao-1	China	2000	1	178	3.38	1.90
Xingo	Brazil	1993	6	140	2.90	1.93

gradually stabilized. Table 7 compares the simulation results with and without considering creep. In Figure 11, the maximum settlement is located in the middle and upper part of the sub-rockfill area of the dam after three years. The settlement of the dam has changed from 75.22 cm to 81.61 cm (0.67% < 1% of the dam height), which reaches a total increase of 8.5%. Both the simulation and monitoring results of Xujixia CFRD are consistent with similar projects in Table 8 and Figure 12.

Figure 13 shows that the simulated maximum settlement of the dam at cross section D0 + 163.8 m agrees well with the measured values. Large settlement occurs rapidly during the construction stage and small settlement occurs in the long term due to creep deformation. Three settlements of measurement points of CS1-2-01, CS1-2-02, and CS1-3-03 are plotted in Figure 13. Large settlement occurs at points CS1-2-02 and S1-3-03, which are close to upstream of the dam due to the influence of water pressure.

The creep deformation at the main rockfill zone generally stabilized after 1-2 years after construction, resulting

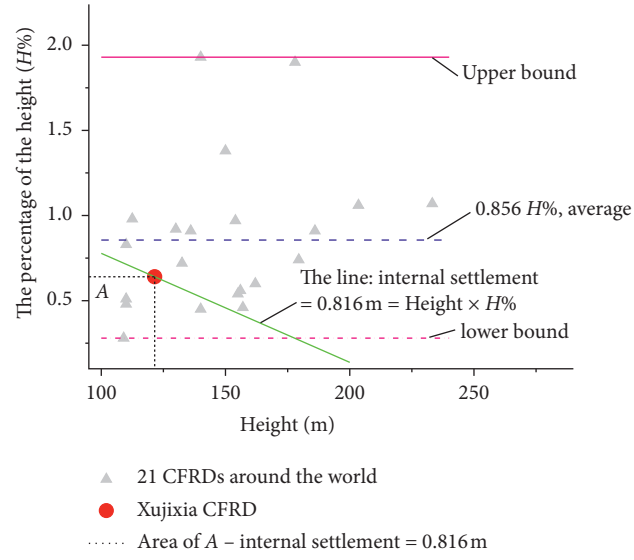

Figure 12: Comparison of the settlement of the Xujixia CFRD and other 100-meter high CFRDs.

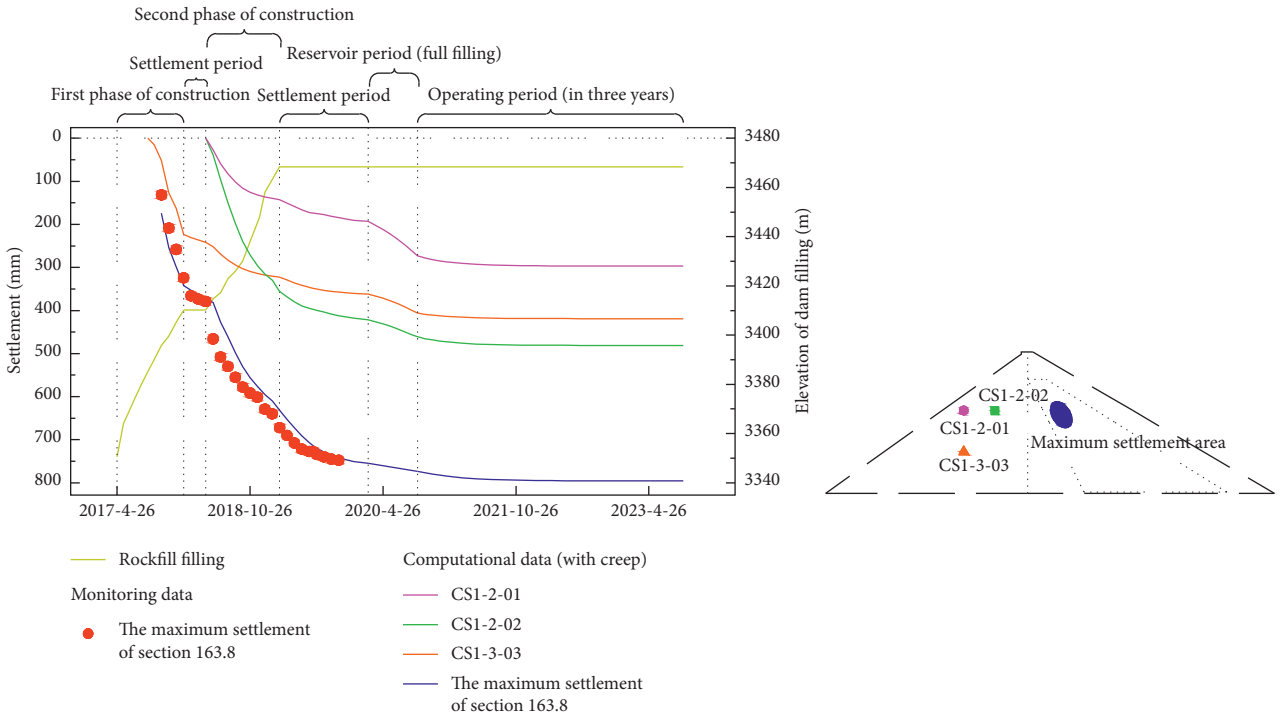

Figure 13: The settlement monitoring results of Xujixia CFRD project.

in more compacted rockfill and increased strength of the dam body. By contrast, the secondary rockfill zone takes a longer time for creep to occur, which is due to the low strength of the rock in this zone. Therefore, particle breakage, slippage, and filling of gaps continue to develop in the secondary rockfill zone.

6. Summary and Conclusions

An UMAT subroutine in ABAQUS was developed based on exponential decay empirical creep model. The creep parameters were obtained by quasilinearization method (BP-MPGA/MPGA) inversion. Numerical simulations were performed based on the Xujixia CFRD project to validate the UMAT subroutine. It was shown that the exponential decay-type empirical creep model was applicable for creep analysis of high CFRDs. Based on the results, the effects of rockfill creep on stress and deformation of the dam were analyzed.

By considering rockfill creep in FEM simulation, the major principal stress (σ_1) and the difference of principal stress ($\sigma_1 - \sigma_3$) were reduced. The stress distribution in the dam tended to be more uniform due to the stress relaxation after creep. By simulating dam body after water storage for three years, the maximum settlement of the Xujixia CFRD increased from 75.22 cm to 81.61 cm by considering dam body creep. Compared with similar projects (100-meter high CFRDs), the Xujixia CFRD has better deformation control effect. Due to the low strength of filling stone, the creep of secondary rockfill zone had a greater impact on stress and deformation distribution of the dam compared with primary rockfill zone.

Data Availability

The data used to support the findings of this study are available from the corresponding author upon request.

Conflicts of Interest

The authors declare that they have no conflicts of interest regarding the publication of this paper.

Acknowledgments

This research was supported by the programme "Creep Analysis and Panel Structure Safety Evaluation of Xujixia CFRD." The authors are grateful to construction management bureau of the Xujixia water conservancy project in Haixi prefecture for providing in situ observation data.

References

[1] J. B. Cooke, "Progress in rockfill dams," *Journal of Geotechnical Engineering Division ASCE*, vol. 110, no. 10, pp. 1383–1414, 1984.

[2] X. Wu, X.-W. Jiang, Y.-F. Chen, H. Tian, and N.-X. Xu, "The influences of mining subsidence on the ecological environment and public infrastructure: a case study at the Haolaigou iron ore mine in Baotou, China," *Environmental Earth Sciences*, vol. 59, no. 4, p. 803, 2009.

[3] C. Silvani, T. Désoyer, and S. Bonelli, "Discrete modelling of time-dependent rockfill behaviour," *International Journal for Numerical and Analytical Methods in Geomechanics*, vol. 33, no. 5, pp. 665–685, 2009.

[4] R. P. Clements, "Post-construction deformation of rockfill dams," *Journal of Geotechnical Engineering*, vol. 110, no. 7, pp. 821–840, 1984.

[5] V. Gikas and M. Sakellariou, "Settlement analysis of the Mornos earth dam (Greece): evidence from numerical modeling and geodetic monitoring," *Engineering Structures*, vol. 30, no. 11, pp. 3074–3081, 2008.

[6] H. Cetin, M. Laman, and A. Ertunç, "Settlement and slaking problems in the world's fourth largest rock-fill dam, the Ataturk Dam in Turkey," *Engineering Geology*, vol. 56, no. 3-4, pp. 225–242, 2000.

[7] B. Zhang, J. G. Wang, and R. Shi, "Time-dependent deformation in high concrete-faced rockfill dam and separation between concrete face slab and cushion layer," *Computers and Geotechnics*, vol. 31, no. 7, pp. 559–573, 2004.

[8] W. Zhou, J. Hua, X. Chang, and C. Zhou, "Settlement analysis of the Shuibuya concrete-face rockfill dam," *Computers and Geotechnics*, vol. 38, no. 2, pp. 269–280, 2011.

[9] Y. Arici, "Investigation of the cracking of CFRD face plates," *Computers and Geotechnics*, vol. 38, no. 7, pp. 905–916, 2011.

[10] Y.-S. Yoon, J.-P. Won, S.-K. Woo, and Y.-C. Song, "Enhanced durability performance of fly ash concrete for concrete-faced rockfill dam application," *Cement and Concrete Research*, vol. 32, no. 1, pp. 23–30, 2002.

[11] D. Liu, X. Zhou, K. Yang, and C. Hua, "Study on siltation self-healing watertight structure for super high CFRD," *Journal of Hydraulic Engineering*, vol. 32, no. 1, pp. 0076–0081, 2001, in Chinese.

[12] Z. Wang, S. Liu, L. Vallejo, and L. Wang, "Numerical analysis of the causes of face slab cracks in Gongboxia rockfill dam," *Engineering Geology*, vol. 181, pp. 224–232, 2014.

[13] S. Siddiqua, J. A. Blatz, and N. C. Privat, "Evaluating turbulent flow in large rockfill," *Journal of Hydraulic Engineering*, vol. 137, no. 11, pp. 1462–1469, 2011.

[14] M. Zhou, B. Zhang, C. Peng, and B. Ronaldo, "Numerical evaluation of soft inter-slab joint in concrete-faced rockfill dam with dual mortar finite element method," *International Journal for Numerical and Analytical Methods in Geomechanics*, vol. 42, no. 5, pp. 781–805, 2018.

[15] Y. Q. Shi, J. J. Yang, J. L. Wu, and J. P. He, "A statistical model of deformation during the construction of a concrete face rockfill dam," *Structural Control and Health Monitoring*, vol. 25, no. 2, Article ID e2074, 2018.

[16] M.-Z. Zhou, B.-y. Zhang, and Y.-x. Jie, "Numerical simulation of soft longitudinal joints in concrete-faced rockfill dam," *Soils and Foundations*, vol. 56, no. 3, pp. 379–390, 2016.

[17] Z. Shi, Z. Wu, C. Gu et al., "Methods for the permeability coefficient of concrete face rockfill dam with cracks," *Advances in Civil Engineering*, vol. 2019, Article ID 6571092, 13 pages, 2019.

[18] Z. Z. Yin, J. G. Zhu, J. P. Yuan, and K. Y. Zhang, "Hydraulic fracture analysis of rock-fill dam with core wall," *Journal of Hydraulic Engineering*, vol. 11, pp. 1348–1353, 2006, in Chinese.

[19] Q. Chen and L. M. Zhang, "Three-dimensional analysis of water infiltration into the Gouhou rockfill dam using saturated–unsaturated seepage theory," *Canadian Geotechnical Journal*, vol. 43, no. 5, pp. 449–461, 2006.

[20] B. Xu, D. Zou, and H. Liu, "Three-dimensional simulation of the construction process of the Zipingpu concrete face rockfill dam based on a generalized plasticity model," *Computers and Geotechnics*, vol. 43, pp. 143–154, 2012.

[21] A. Gurbuz, "A new approximation in determination of vertical displacement behavior of a concrete-faced rockfill dam," *Environmental Earth Sciences*, vol. 64, no. 3, p. 883, 2011.

[22] G. T. Liu, H. U. Yu, X. G. Jiao, and L. I. Peng-Hui, "Stress analysis of concrete slab in high CFRD and measures for improving the stress state," *Journal of Hydraulic Engineering*, vol. 37, no. 2, pp. 135–140, 2006, in Chinese.

[23] S. C. Anna, C. Adam, and M. Michel, "Use of deformation monitoring results in solving geomechanical problems—case studies," *Engineering Geology*, vol. 79, no. 1-2, pp. 3–12, 2005.

[24] R. Sukkarak, P. Jongpradist, and P. Pramthawee, "A modified valley shape factor for the estimation of rockfill dam settlement," *Computers and Geotechnics*, vol. 108, pp. 244–256, 2019.

[25] M. Karalar and M. Çavuşli, "Seismic effects of epicenter distance of earthquake on 3D damage performance of CG dam," *Earthquakes and Structures*, vol. 18, no. 2, pp. 201–213, 2020.

[26] M. Karalar and M. Çavuşli, "Assessing 3D seismic damage performance of a CFR dam considering various reservoir heights," *Earthquakes and Structures*, vol. 16, no. 2, pp. 221–234, 2019.

[27] M. Karalar and M. Çavuşli, "Evaluation of 3D nonlinear earthquake behaviour of ilisu CFR dam under far fault ground motions," *Advances in Civil Engineering*, vol. 2019, Article ID 7358710, 15 pages, 2019.

[28] R. Kuwano and R. J. Jardine, "On measuring creep behaviour in granular materials through triaxial testing," *Canadian Geotechnical Journal*, vol. 39, no. 5, pp. 1061–1074, 2002.

[29] W. Zhou, X. L. Chang, C. B. Zhou, and X. H. Liu, "Creep analysis of high concrete-faced rockfill dam," *International Journal for Numerical Methods in Biomedical Engineering*, vol. 26, no. 11, pp. 1477–1492, 2010.

[30] X. X. Zhou, S. C. Chi, M. H. Wang, and Y. F. Jia, "Study on wetting deformation characteristics of coarse granular materials and its simulation in core-wall rockfill dams," *International Journal for Numerical and Analytical Methods in Geomechanics*, vol. 44, no. 6, pp. 851–873, 2020.

[31] J. Liang, H. L. Liu, and Y. F. Gao, "Study and inversion of rheological properties of rockfill," *Journal of Seismology*, vol. 24, no. 1, pp. 77–81, 2004.

[32] D. Li, Z. Sun, T. Xie, X. Li, and P. G. Ranjith, "Energy evolution characteristics of hard rock during triaxial failure with different loading and unloading paths," *Engineering Geology*, vol. 228, pp. 270–281, 2017.

[33] W. Zhou, Y. Chen, G. Ma, L. Yang, and X. Chang, "A modified dynamic shear modulus model for rockfill materials under a wide range of shear strain amplitudes," *Soil Dynamics and Earthquake Engineering*, vol. 92, pp. 229–238, 2017.

[34] B. Y. Zhang, J. H. Zhang, and G. L. Sun, "Deformation and shear strength of rockfill materials composed of soft siltstones subjected to stress, cyclical drying/wetting and temperature variations," *Engineering Geology*, vol. 190, pp. 87–97, 2015.

[35] J. Herrmann, E. Rybacki, H. Sone, and G. Dresen, "Deformation experiments on bowland and posidonia shale-part II: creep behavior at in situ pc-T conditions," *Rock Mechanics and Rock Engineering*, vol. 53, no. 2, pp. 755–779, 2019.

[36] Q. Sun, Y. G. Cai, J. Chu, Q. Y. Dong, and J. Wang, "Effect of variable confining pressure on cyclic behaviour of granular soil under triaxial tests," *Canadian Geotechnical Journal*, vol. 54, no. 6, 2017.

[37] C. Morin, T. Sedran, F. de Larrard et al., "Development of an excavatability test for backfill materials: numerical and experimental studies," *Canadian Geotechnical Journal*, vol. 55, no. 1, 2018.

[38] E. E. Alonso and M. A. Tapias, "Suction and time effects in rockfill deformation," *International Journal for Numerical and Analytical Methods in Geomechanics*, vol. 43, no. 5, pp. 1032–1050, 2019.

[39] T. Xu, Q. Xu, M. Deng, T. Ma, T. Yang, and C.-a. Tang, "A numerical analysis of rock creep-induced slide: a case study from Jiweishan Mountain, China," *Environmental Earth Sciences*, vol. 72, no. 6, pp. 2111–2128, 2014.

[40] E. L. Liu, Y. L. Tan, S. S. Chen, and G. Y. Li, "Investigation on critical state of rockfill materials," *Journal of Hydraulic Engineering*, vol. 43, no. 5, pp. 505–511, 2012, in Chinese.

[41] G. Sun, Y. Huang, C. Li, and H. Zheng, "Formation mechanism, deformation characteristics and stability analysis of Wujiang landslide near Centianhe reservoir dam," *Engineering Geology*, vol. 211, pp. 27–38, 2016.

[42] G. Ma, W. Zhou, T.-T. Ng, Y.-G. Cheng, and X.-L. Chang, "Microscopic modeling of the creep behavior of rockfills with a delayed particle breakage model," *Acta Geotechnica*, vol. 10, no. 4, pp. 481–496, 2015.

[43] Y. Xiao, L. Long, T. M. Evans, H. Zhou, H. Liu, and A. W. Stuedlein, "Effect of particle shape on stress-dilatancy responses of medium-dense sands," *Journal of Geotechnical & Geoenvironmental Engineering*, vol. 145, no. 2, Article ID 04018105, 2019.

[44] Y. Xiao, Z. X. Yuan, S. Desai Chandrakant et al., "Effects of load duration and stress level on deformation and particle breakage of carbonate sands," *International Journal of Geomechanics*, vol. 20, no. 7, Article ID 06020014, 2020.

[45] G. Lei, Z. Z. Shen, and L. Q. Xu, "Long-term deformation analysis of the jiudianxia concrete-faced rockfill dam," *Arabian Journal for Science & Engineering*, vol. 39, no. 3, pp. 1589–1598, 2014.

[46] M. Karalar and M. Çavuşli, "Examination of 3D long-term viscoplastic behaviour of a CFR dam using special material models," *Geomechanics and Engineering*, vol. 17, no. 2, pp. 119–131, 2019.

[47] Z. Li, T. S. Nguyen, G. Su, D. Labrie, and J. D. Barnichon, "Development of a viscoelastoplastic model for a bedded argillaceous rock from laboratory triaxial tests," *Canadian Geotechnical Journal*, vol. 54, no. 3, pp. 359–372, 2017.

[48] Y. F. Chen, R. Hu, W. B. Lu, D. Q. Li, and C. B. Zhou, "Modeling coupled processes of non-steady seepage flow and non-linear deformation for a concrete-faced rockfill dam," *Computers & Structures*, vol. 89, no. 13-14, pp. 1333–1351, 2011.

[49] P. Pramthawee, P. Jongpradist, and R. Sukkarak, "Integration of creep into a modified hardening soil model for time-dependent analysis of a high rockfill dam," *Computers and Geotechnics*, vol. 91, pp. 104–116, 2017.

[50] Y. Kong, M. Xu, and E. Song, "An elastic-viscoplastic double-yield-surface model for coarse-grained soils considering particle breakage," *Computers and Geotechnics*, vol. 85, pp. 59–70, 2017.

[51] M. Wang, Y. F. Chen, R. Hu, W. Liu, and C. B. Zhou, "Coupled hydro-mechanical analysis of a dam foundation with thick fluvial deposits: a case study of the Danba hydropower project, Southwestern China," *Revue Française de Génie Civil*, vol. 20, no. 1, p. 26, 2016.

[52] Y. Xiao and H. Liu, "Elastoplastic constitutive model for rockfill materials considering particle breakage," *International Journal of Geomechanics*, vol. 17, no. 1, Article ID 04016041, 2017.

[53] L. Wen, J. Chai, Z. Xu, Y. Qin, and Y. Li, "Monitoring and numerical analysis of behaviour of Miaojiaba concrete-face rockfill dam built on river gravel foundation in China," *Computers and Geotechnics*, vol. 85, pp. 230–248, 2017.

[54] J. M. Duncan, P. Byrne, K. Wong, and P. Mabry, *Strength, Stress-Strain and Bulk Modulus Parameters for Finite Element Analysis of Stresses and Movements in Soil Masses*, UCB/GT/80-01 University of California, Berkeley, CA, USA, 1980.

[55] K. M. Wei and S. Zhu, "A generalized plasticity model to predict behaviors of the concrete-faced rock-fill dam under complex loading conditions," *European Journal of Environmental and Civil Engineering*, vol. 17, no. 7, pp. 579–597, 2013.

[56] Y. Yu, B. Zhang, and H. Yuan, "An intelligent displacement back-analysis method for earth-rockfill dams," *Computers and Geotechnics*, vol. 34, no. 6, pp. 423–434, 2007.

[57] M. Rashidi and S. M. Haeri, "Evaluation of behaviors of earth and rockfill dams during construction and initial impounding using instrumentation data and numerical modeling," *Journal of Rock Mechanics and Geotechnical Engineering*, vol. 9, no. 4, pp. 709–725, 2017.

[58] F.-h. Yao, S.-h. Guan, H. Yang et al., "Long-term deformation analysis of Shuibuya concrete face rockfill dam based on response surface method and improved genetic algorithm," *Water Science and Engineering*, vol. 12, no. 3, pp. 196–204, 2019.

[59] W. Zhou and X. L. Chang, "Creep analysis of high concrete faced rockfill dam based on creep constitutive model of power function," *Journal of Hydroelectric Engineering*, vol. 25, no. 1, p. 15, 2006, in Chinese.

[60] J. L. Justo and P. Durand, "Settlement-time behaviour of granular embankments," *International Journal for Numerical and Analytical Methods in Geomechanics*, vol. 24, no. 3, pp. 281–303, 2000.

[61] D. W. Taylor and W. Merchant, "A theory of clay consolidation accounting for secondary compression," *Journal of Mathematics and Physics*, vol. 19, no. 1–4, pp. 167–185, 1940.

[62] Z. J. Shen and K. Z. Zhao, "Feedback analysis of creep deformation of rockfill dam," *Journal of Hydraulic Engineering*, vol. 6, no. 6, pp. 2–7, 1998, in Chinese.

[63] Z. J. Shen, "Creep model of earth and stone and its application," *Scientific Research on Water Resources and Water Transport*, vol. 4, no. 4, pp. 335–342, 1994, in Chinese.

[64] G. Li, Z. Mi, H. Fu, and W. Fang, "Experimental studies on rheological behaviors for rockfills in concrete faced rockfill dam," *Rock Soil Mechanics*, vol. 25, no. 11, pp. 1712–1716, 2004, in Chinese.

[65] Y. Y. Huang, Z. Z. Shen, H. Zheng, and C. G. Li, "A note on three-dimensional rheological rate of rockfill," *Rock and Soil Mechanics*, vol. 35, no. 6, pp. 1569–1571, 2014, in Chinese.

[66] R. E. Goodman, R. L. Taylor, and T. L. Brekke, "A model for the mechanics of jointed rock," *Journal of Soil Mechanics and Foundation Division ASCE*, vol. 94, no. 3, pp. 637–659, 1968.

[67] G. W. Clough and J. M. Duncan, "Finite element analysis of retaining wall behavior," *Journal of Soil Mechanics and Foundation Engineering*, vol. 97, no. 12, pp. 1657–1672, 1971.

[68] P. Guo and W.-c. Li, "Development and implementation of Duncan-Chang constitutive model in GeoStudio2007," *Procedia Engineering*, vol. 31, pp. 395–402, 2012.

[69] X.-q. Liu, J.-k. Liu, Y.-h. Tian, D. Chang, and T.-f. Hu, "Influence of the freeze-thaw effect on the Duncan-Chang model parameter for lean clay," *Transportation Geotechnics*, vol. 21, p. 100273, 2019.